Analyst

RSC Publishing

PAPER

View Article Online
View Journal | View Issue

Cite this: *Analyst*, 2013, **138**, 2931

Simple pyridyl-salicylimine-based fluorescence "turn-on" sensors for distinct detections of Zn^{2+}, Al^{3+} and OH^- ions in mixed aqueous media†

Muthaiah Shellaiah, Yen-Hsing Wu and Hong-Cheu Lin*

Received 12th December 2012
Accepted 5th March 2013

DOI: 10.1039/c3an36840h

www.rsc.org/analyst

Simple pyridyl-salicylimine derivatives (**F1**, **F2** and **F3**) are reported for the first time as fluorescence "turn-on" sensors for distinct detections of Zn^{2+}, Al^{3+} and OH^- ions in mixed-aqueous media CH_3CN/H_2O with volume ratios of 6/4 and 3/7 (at pH = 7 and 25 °C) *via* internal charge transfer (ICT), chelation enhanced fluorescence (CHEF), and deprotonation mechanisms. **F1** and **F2** show diverse turn-on sensing applications to Zn^{2+}, Al^{3+} and OH^- ions, but **F3** exhibited the fluorescence turn-on sensing to Al^{3+} and OH^- ions in CH_3CN/H_2O (6/4; vol/vol). **F1**+Zn^{2+} and **F2**+Zn^{2+} complexes revealed the reversibilities and ratiometric displacements of Zn^{2+} with ethylene diamine tetra acetic acid (EDTA) and Al^{3+} ions, respectively, in CH_3CN/H_2O (6/4; vol/vol). On the other hand, **F1**, **F2** and **F3** in CH_3CN/H_2O (3/7; vol/vol) showed sensitivities only to Al^{3+} ions but negligible selectivities to OH^- ions. Stoichiometry of all sensor complexes were calculated as 1 : 1 by job's plots based on UV/Vis and PL titrations. The complex formation and binding sites of all sensor materials were well characterized by ^1H, ^{13}C NMR, and mass (FAB) spectral analysis. Detection limits were calculated from standard deviations and linear fitting calculations. The association constant (log K_a) values of sensor complexes were evaluated from the fluorescence binding isotherms. The fluorescence decay constant (τ) values were estimated from time resolved fluorescence studies. Time, temperature, pH and solvent concentration effects towards sensor responses were fully investigated in this report.

Introduction

The design and synthesis of new molecular sensors towards biologically and environmentally important species are always essential for practical research in various fields of science.[1] Among the available detection methods, chemosensors based on ion-induced fluorescence changes are predominantly attractive in terms of sensitivity, selectivity, response time, simplicity, high degree of specificity and low detection limit.[2] Due to the fluorescence quenching effects[3] of biologically important ions, the developments of fluorescence turn-on sensors still remains a challenging task. Hence, several molecular turn-on sensors[4] were reported for a variety of cations and anions based on photo induced electron transfer (PET), internal charge transfer (ICT), chelation enhanced fluorescence (CHEF), and deprotonation mechanisms. Among them, PET[5] exhibited various changes of emission intensities with some or no spectral shifts, whereas ICT[6] caused both intensity changes and spectral shifts, and CHEF[7] also provided fluorescence enhancements with or without any spectral changes.

In the midst of the important heavy metal ions in the human body, zinc is the second most abundant metal ion and is actively involved in diverse biological activities, such as structural and catalytic cofactors, neural signal transmitters or modulators, regulators of gene expression and apoptosis.[8] Minute quantities of zinc are necessary for the living organism, but excessive amounts may damage the organism.[9] Additionally, to the best of our knowledge, some available Zn^{2+} sensors[10] have difficulty in distinguishing Zn^{2+} from Cd^{2+}, since cadmium is in the same group of the periodic table and has similar properties. Therefore, the design of a highly selective and sensitive fluorescence sensor for Zn^{2+} detection without interference from other metal ions, especially Cd^{2+}, is one of the most important objectives. On the other hand, aluminum is the third most prevalent (8.3% by weight) metallic element on the earth and its soluble form (Al^{3+}) is highly toxic to plant growth.[11] Intemperance of Al^{3+} deposition in the brain is believed to cause neurodementia, such as Parkinson's disease, Alzheimer's disease, and dialysis encephalopathy.[12] However, owing to the weak coordination and strong hydration ability of Al^{3+} in water, it is easily interfered by the variations of the pH values in solution and the coexistence of interfering ions.[13] In comparison with transition-metal ions,

Department of Materials Science and Engineering, National Chiao Tung University, Hsinchu 30049, Taiwan (ROC). E-mail: linhc@mail.nctu.edu.tw

† Electronic supplementary information (ESI) available: For synthesis and sensor characterization by UV/PL, ^{13}C NMR and mass (FAB) spectral evidences. See DOI: 10.1039/c3an36840h

scarce examples of fluorescence sensors have been reported for Al^{3+} so far and most of them have synthetic difficulties with limited sensitivities or selectivities. Therefore, it is highly desirable to develop more sophisticated and selective Al^{3+} sensors which can be easily synthesized and handled.[14]

Similarly, hydroxide ions are ubiquitous in nature, and their properties are important in chemical, biological, environmental, and atmospheric processes.[15] Hydroxide is used worldwide in many industrial processes, and rapid and reliable methodologies for the sensing of hydroxide ions for quality control purposes and monitoring during industrial processing are required.[16] Problems arise quite simply due to the corrosive nature of the alkali and glass, so pH electrodes become insensitive and unstable at high concentrations.[17] Hence, selective sensors of hydroxide ions at higher pHs are favorable. Owing to the importance of Zn^{2+}, Al^{3+} and OH^- ions, many sensory reports for them are separately available as mentioned previously, but sensor probes with dissimilar responses to those analytes are cost-effective and highly desirable for real time applications. However, developments of such sensors are challenging tasks and also have the synthetic difficulties.[18] In these considerations, Schiff bases[19] were reported as sensory materials for various analytes with least synthetic difficulties, but only a few of them were accounted for by multiple analyte recognitions.[20]

Herein, for the first time we report pyridyl-salicylimine[21] Schiff base derivatives (**F1**, **F2** and **F3**) as fluorescence "turn-on" sensors for distinct detections of Zn^{2+}, Al^{3+} and OH^- ions in mixed-aqueous media [CH_3CN/H_2O (6/4 and 3/7; vol/vol), pH = 7 and at 25 °C] *via* ICT, CHEF and deprotonation mechanisms as illustrated in Fig. 1.

Results and discussion

Synthesis and photophysical properties

Three pyridyl-salicylimine Schiff base derivatives **F1**, **F2** and **F3** (Fig. 1) were easily synthesized *via* one-pot aldehyde–amine condensation[22] reaction as noticed in Scheme S1,† in the presence of methanol with excellent yields and high purities. The photophysical properties and sensor responses of **F1**, **F2** and **F3** are shown in Table 1. The absorption and PL maxima of **F1**, **F2** and **F3**, are 344, 346, 343 nm, and 424, 427, 432 nm, respectively. The quantum yield (Φ) measurements were carried out at different mixed-aqueous media (CH_3CN/H_2O) concentrations. Even though, the quantum yields of **F1**, **F2** and **F3** were evidenced that they can be used for sensor applications in CH_3CN/H_2O at 6/4, 1/1 and 3/7 vol ratios, but we tend to choose higher and lower vol ratios (6/4 and 3/7) of mixed-aqueous media. Hence, initially we carried out the sensor titrations in CH_3CN/H_2O (6/4; vol/vol), and then we extended to CH_3CN/H_2O (3/7; vol/vol). Similarly, the pH measurements of **F1**, **F2** and **F3** (Fig. S10 and S11; see the ESI†) suggested that they can be utilized for the sensor titrations from pH = 0 to pH = 8. However, TRPL studies of **F1**, **F2** and **F3** at acidic pHs affected their fluorescence decay constants (Fig. S12 and Table S2; see the ESI†). Therefore, we performed all of our UV-Vis/PL titrations in CH_3CN/H_2O (6/4 and 3/7; vol/vol), pH = 7 and at 25 °C. On the other hand, to evaluate the sensor responses, the ^1H and ^{13}C NMR titrations were carried out by dissolving **F1**, **F2** and **F3** in CD_3CN and other ions (Zn^{2+}, Al^{3+} and OH^-) in D_2O.

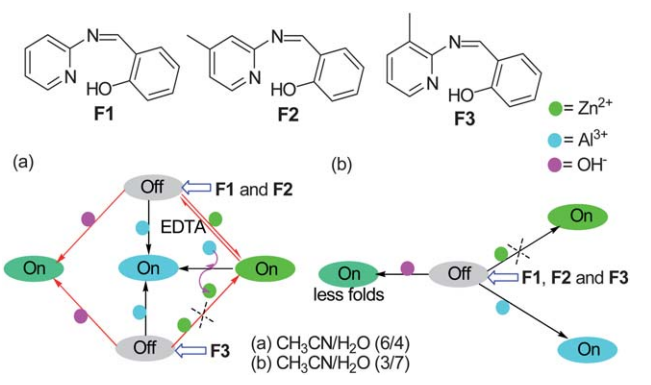

Fig. 1 Structures and schematic representations of sensor responses of **F1**, **F2** and **F3** in (a) CH_3CN/H_2O (6/4; vol/vol) and (b) CH_3CN/H_2O (3/7; vol/vol).

HOMO–LUMO calculations

The HOMO–LUMO calculations of **F1**, **F2** and **F3** were carried out by semi-empirical AM1 method[23] and we found that HOMO and LUMO of **F1** and **F3** were localized on phenyl and pyridyl rings, respectively, whereas, for **F2** both HOMO and LUMO were located equally on phenyl and pyridyl rings as noticed in Fig. S13A–C.† However, the above case was not observed in phenoxides of **F1**, **F2** and **F3**, in which the phenoxides of **F2** and **F3** positioned their HOMO and LUMO in phenyl and pyridyl rings, respectively, and **F1** sited them only on phenyl rings as shown in Fig. S13D–F.† The localization of electron clouds in **F1**, **F2** and **F3** were also affected during the formation of sensor complexes and the formation of phenoxides were highly favourable at higher pHs. Therefore, this calculation provides more support for lateral explanations of sensor complexes of **F1**, **F2** and **F3** with Zn^{2+} and Al^{3+} ions as well as phenoxide formed of **F1–F3** with OH^- ions.

Fluorescence titrations on cations and anions

Initially, **F1**, **F2** and **F3** in CH_3CN/H_2O (6/4; vol/vol) were investigated towards metal ions (Li^+, Ag^+, K^+, Na^+, Cs^+, Ni^{2+}, Fe^{2+}, Co^{2+}, Zn^{2+}, Cd^{2+}, Pb^{2+}, In^{3+}, Ga^{3+}, Mg^{2+}, Cu^{2+}, Cr^{3+}, Fe^{3+}, Ag^{2+}, Mn^{2+}, Eu^{3+}, Hg^{2+}, Mg^{2+} and Al^{3+} in H_2O), and then extended to CH_3CN/H_2O (3/7; vol/vol). As shown in Fig. 2, **F1** and **F2** revealed selectivities to Zn^{2+} and Al^{3+} ions with different spectral shifts, but **F3** showed the selectivity just to Al^{3+} ions with no sensor response to Zn^{2+} ions. Due to the ICT mechanism, **F1** and **F2** exhibited with different spectral shifts towards Zn^{2+} and Al^{3+} ion PL enhancements. However, in **F3** the ICT found to be inhibited by the presence of methyl group in the third position of the pyridyl unit, and hence provided selectivity just to Al^{3+} ions *via* CHEF mechanism. The PL maxima of **F1**+Zn^{2+}, **F2**+Zn^{2+}, **F1**+Al^{3+}, **F2**+Al^{3+} and **F3**+Al^{3+} appeared at 508, 505, 487, 485 and 477 nm, respectively, with more folds of PL enhancements. As shown in Table 1, the sensor properties and PL intensities of **F1**, **F2** and **F3** to Zn^{2+} demonstrated a

Table 1 Photophysical and sensor properties of **F1**, **F2** and **F3**

Compound	Φ	Sensor response to Zn^{2+a}	Sensor response to Al^{3+a}	Sensor response to OH^{-a}	$\tau^{a,b,c,e}$ (ns)
F1 (λ_{ex} = 344 nm; λ_{em} = 424 nm)	0.011[a] 0.016[b] 0.018[c] 0.033[d]	Turn-on (29.9 folds) (λ_{ex} = 344 nm; λ_{em} = 508 nm)	Turn-on (29.5 folds) (λ_{ex} = 344 nm; λ_{em} = 487 nm)	Turn-on (30.1 folds) (λ_{ex} = 344 nm; λ_{em} = 502 nm)	2.19
F2 (λ_{ex} = 346 nm; λ_{em} = 427 nm)	0.008[a] 0.012[b] 0.014[c] 0.030[d]	Turn-on (29.2 folds) (λ_{ex} = 346 nm; λ_{em} = 505 nm)	Turn-on (39 folds) (λ_{ex} = 346 nm; λ_{em} = 485 nm)	Turn-on (19.7 folds) (λ_{ex} = 346 nm; λ_{em} = 499 nm)	1.51
F3 (λ_{ex} = 343 nm; λ_{em} = 432 nm)	0.010[a] 0.013[b] 0.015[c] 0.031[d]	NA	Turn-on (44.8 folds) (λ_{ex} = 343 nm; λ_{em} = 477 nm)	Turn-on (22.9 folds) (λ_{ex} = 343 nm; λ_{em} = 500 nm)	1.35

[a] CH_3CN/H_2O (10–6/0–4; vol/vol). [b] CH_3CN/H_2O (1/1; vol/vol). [c] CH_3CN/H_2O (3/7; vol/vol). [d] CH_3CN/H_2O (1/99; vol/vol), 9,10-diphenyl anthracene (DPA) in CH_3CN as a reference standard (Φ = 0.9). [e] Fluorescence lifetimes.

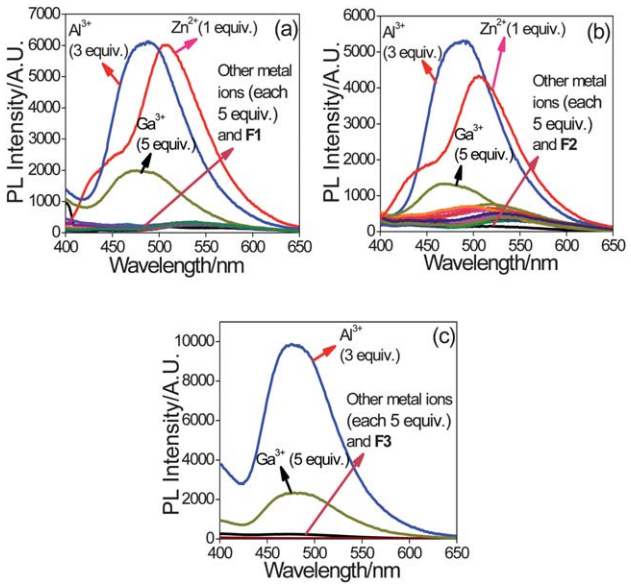

Fig. 2 Sensor responses of (a) **F1** in CH_3CN/H_2O (6/4; vol/vol), (b) **F2** in CH_3CN/H_2O (6/4; vol/vol) and (c) **F3** in CH_3CN/H_2O (6/4; vol/vol) towards metal ions in H_2O.

decreasing trend as **F1**+Zn^{2+} > **F2**+Zn^{2+} > **F3**+Zn^{2+} (29.9 and 29.2 folds and no sensitivities). In contrast to the Zn^{2+} sensors, the PL intensities of **F1**, **F2** and **F3** to Al^{3+} pronounced a reverse trend as **F1**+Al^{3+} < **F2**+Al^{3+} < **F3**+Al^{3+} (29.5, 39 and 44.8 folds). Similarly, as visualized in Fig. 4A and B, **F1** and **F2** provides the turn-on sensor responses to Zn^{2+} and Al^{3+} with green and blue fluorescence with differential spectral shifts. On the other hand, **F3** exhibited turn-on sensor response to Al^{3+} with blue fluorescence rather than Zn^{2+} as noticed in Fig. 4C. The above variation could be well explained on the basis of HOMO and LUMO concept (Fig. S13A–C†), wherein both HOMO and LUMO electron clouds were located in both rings of **F2**. Comparing **F1** and **F3**, even though they possessed HOMO and LUMO electron clouds correspondingly on phenyl and pyridyl rings, the presence of methyl group in **F3** provided entirely different sensor properties. Further investigations of **F1**, **F2** and **F3** in CH_3CN/H_2O (6/4; vol/vol) towards various anions (F^-, Br^-, Cl^-, I^-, ClO_4^-, BH_4^-, NO_3^-, PO_4^- and OH^-) in H_2O at pH = 7, 25 °C showed selective sensor responses to OH^- anions as noticed in Fig. 1 and 3. However, their PL intensity changes towards OH^- ions varied as shown in Table 1; **F1**, **F2** and **F3** revealed 30.1, 19.7 and 22.9 folds, respectively, along with green fluorescence under UV-light irradiations as envisaged in Fig. 4A–C. Formation of phenoxide ions might be the cause for the PL enhancements of **F1**, **F2** and **F3**, roughly at *ca.* 500 nm. In addition, the pH value of the above sensor systems to OH^- ions were noticed as 7, even maintained after the PL excitations, and allowed us to accomplish the further measurements such as pH effects. As shown Fig. S13D–F† in HOMO–LUMO levels **F2** and

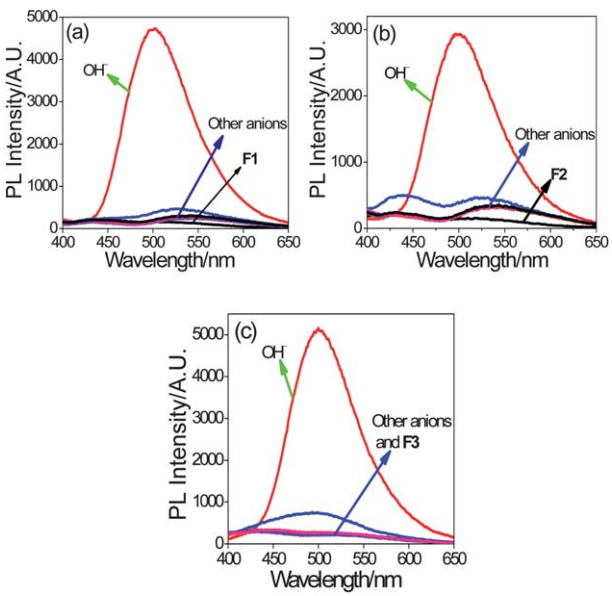

Fig. 3 Sensor responses of (a) **F1** in CH_3CN/H_2O (6/4; vol/vol), (b) **F2** in CH_3CN/H_2O (6/4; vol/vol) and (c) **F3** in CH_3CN/H_2O (6/4; vol/vol) towards anions in H_2O (each 50 equiv.).

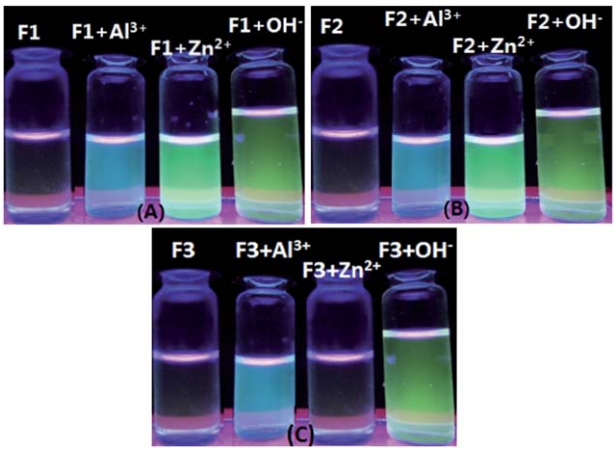

Fig. 4 Photographs of sensor responses of (A) **F1**, (B) **F2** and (C) **F3** upon the addition of Al^{3+} (3 equiv.), Zn^{2+} (1 equiv.) and OH^- (50 equiv.) under UV-light irradiations.

F3-phenoxides were localized on phenyl and pyridyl rings, respectively, but **F1**-phenoxide was restricted just to the phenyl ring. However, the under-sized difference in PL enhancements of **F2** and **F3** to OH^- ions was due to the positional change of methyl substituent in the pyridyl unit. Therefore the sensor responses trend of **F1**, **F2** and **F3** to OH^- ions were akin to **F1**+OH^- > **F3**+OH^- > **F2**+OH^- as noticed in Table 1. The sensor titrations of **F1**, **F2** and **F3** on cations were repeated in CH_3CN/H_2O (3/7; vol/vol), and evidenced the sensitivities of them only to Al^{3+} ions as noticed in Fig. S14 (see the ESI†).

UV-Vis/PL titrations on Zn^{2+} ions

By increasing the concentrations of Zn^{2+} 0–30 μM (0, 2, 4, 6, 8, 10, 14, 16, 18, 20, 22, 24 and 30 μM in H_2O), except **F3**, the sensitivities of **F1** and **F2** (20 μM) in CH_3CN/H_2O (6/4; vol/vol) towards Zn^{2+} ions were clearly observed in Fig. 5. The fluorescence spectra of **F1** (λ_{em} = 508 nm) and **F2** (λ_{em} = 505 nm) showed turn-on responses rapidly, and the insets clearly illustrated that the turn-on properties were saturated at 20 μM Zn^{2+} ions, thereafter further addition of Zn^{2+} affected the sensor property. The above statement was further confirmed *via* stoichiometry, binding site, and sensor complex formation studies. In order to establish the specific selectivities of **F1** and **F2** to Zn^{2+}, we performed the single and dual metal competitive analysis as noticed in Fig. 6. In single metal system (black bars), all the metal ion (Li^+, Ag^+, K^+, Na^+, Cs^+, Ni^{2+}, Fe^{2+}, Co^{2+}, Zn^{2+}, Cd^{2+}, Pb^{2+}, In^{3+}, Ga^{3+}, Mg^{2+}, Cu^{2+}, Cr^{3+}, Fe^{3+}, Ag^{2+}, Mn^{2+}, Eu^{3+}, Hg^{2+}, Mg^{2+} and Al^{3+} in H_2O) concentrations were kept at 20 μM, and for dual-metal (red bars) studies, 20 μM of Zn^{2+} + 20 μM of other metal ions in H_2O and 20 μM of Zn^{2+} + 20 μM of metal ion mixtures in H_2O were taken. During the dual metal analysis, the Zn^{2+} effect at 40 μM was taken and we found that an excess addition of Zn^{2+} would affect the sensitivities as mentioned before. Furthermore, the sensitivities of **F1** and **F2** towards Zn^{2+} ions can be well demonstrated as in Fig. 6, which explains sensing abilities of **F1** and **F2** in the presence of different metal ion backgrounds. Both systems (single and dual-metal analysis)

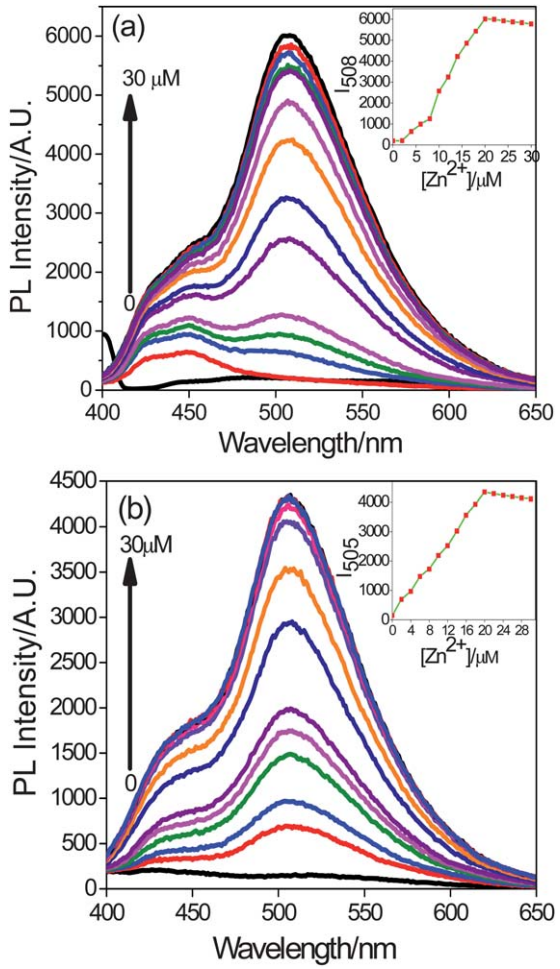

Fig. 5 Fluorescence spectral changes of (a) **F1** (20 μM) in CH_3CN/H_2O (6/4) (λ_{ex} = 344 nm) and (b) **F2** (20 μM) in CH_3CN/H_2O (6/4; vol/vol) (λ_{ex} = 346 nm) titrated with 0–30 μM of Zn^{2+} ions in H_2O (0, 2, 4, 6, 8, 10, 14, 16, 18, 20, 22, 24 and 30 μM were plotted). Insets show PL spectral responses of (a) **F1** and (b) **F2** as a function of Zn^{2+}.

confirmed the sensitivities of **F1** and **F2** to Zn^{2+} even in the presence of interfering Cd^{2+} ions. However, in both cases of **F1** and **F2**, the sensor responses were entirely affected by the presence of Al^{3+} ions rather than the other metal ions. This helped us to perform the ratiometric displacement measurements, to establish the distinguishable selectivities of **F1** and **F2** to both Zn^{2+} and Al^{3+} ions. Additional explanations for the interfering effect of Al^{3+} ions to Zn^{2+} sensor was also provided by the association constant (log K_a) studies. In addition to fluorescence titrations, UV-Vis absorption titrations also revealed the sensitivities of **F1** and **F2** to Zn^{2+} ions. Both **F1** and **F2** exhibited absorption maxima at 344 and 346 nm, respectively, and upon the addition of Zn^{2+} ions 0–30 μM (0, 5, 10, 15, 20, 22, 24, 28 and 30 μM) shows the quenching spectra as evidenced in Fig. S15 (see the ESI†).

UV-Vis/PL titrations on Al^{3+} ions

Upon the addition of Al^{3+} 0–60 μM (0, 5, 10, 15, 20, 25, 30, 35, 45, 50, 55 and 60 μM in H_2O), **F1** and **F2** (20 μM) in CH_3CN/H_2O (6/

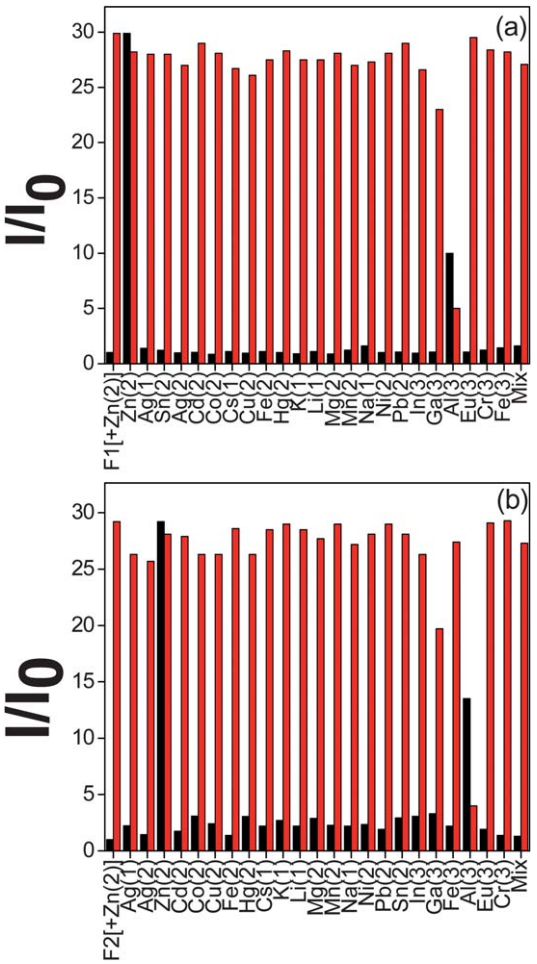

Fig. 6 Relative fluorescence intensities of (a) **F1** (20 μM) and (b) **F2** (20 μM) in CH_3CN/H_2O (6/4; vol/vol) with 20 μM Zn^{2+} in H_2O in the presence of competing metal ions. Black bars; **F1** and **F2** (20 μM) in CH_3CN/H_2O (6/4; vol/vol) with 20 μM of stated metal ions in H_2O. Red bars; **F1** and **F2** (20 μM) CH_3CN/H_2O (6/4; vol/vol) with 20 μM Zn^{2+} + 20 μM of stated metal ions in H_2O (40 μM of Zn^{2+} for Zn^{2+} effect) (mix = combinations of all metal ions except Zn^{2+} and Al^{3+}).

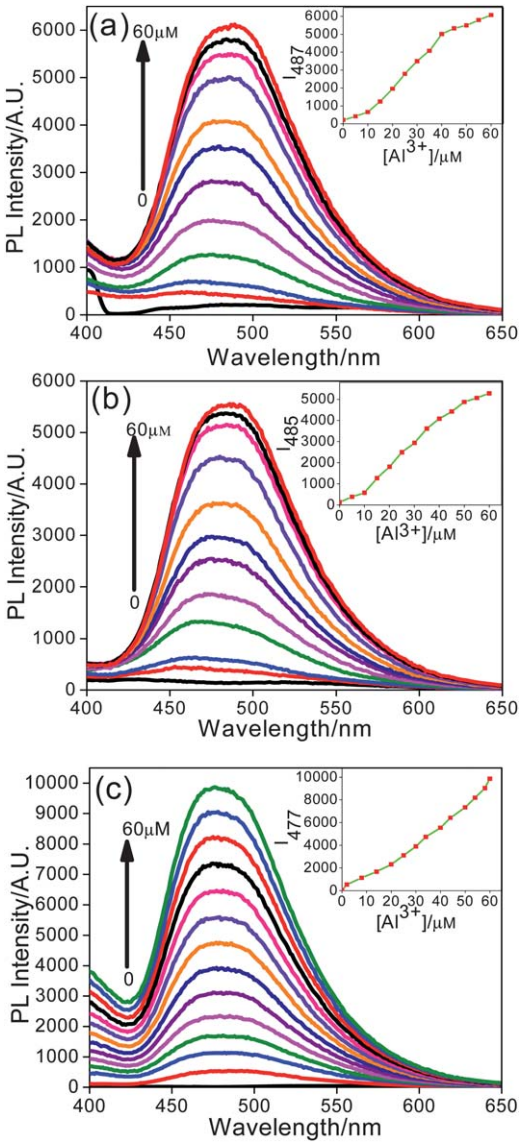

Fig. 7 Fluorescence spectral changes of (a) **F1** (1×10^{-5} M) in CH_3CN/H_2O (6/4; vol/vol) (λ_{ex} = 344 nm), (b) **F2** (1×10^{-5} M) in CH_3CN/H_2O (6/4; vol/vol) (λ_{ex} = 346 nm), and (c) **F3** (1×10^{-5} M) in CH_3CN/H_2O (6/4; vol/vol) (λ_{ex} = 343 nm) titrated with 0–60 μM of Al^{3+} ions in H_2O (0, 5, 10, 15, 20, 25, 30, 35, 45, 50, 55 and 60 μM were plotted for **F1** and **F2**, along with **F3** was plotted with an equal span of 5 μM). Insets show PL spectral responses of (a) **F1**, (b) **F2** and (c) **F3** as a function of Al^{3+}.

4; vol/vol) revealed selectivities with appearances of emission peaks (Fig. 7a and b) at 487 and 485 nm, respectively. In the same way, **F3** (20 μM) in CH_3CN/H_2O (6/4; vol/vol) also indicated its sensitivity to Al^{3+} (0–60 μM with an equal span of 5 μM) through the appearance of peaks at 477 nm, as noticed in Fig. 7c. The insets showed the PL intensity changes with respect to the concentration of Al^{3+}, and also confirmed that an excess addition of Al^{3+} did not affect the sensitivity. In addition, the selectivities of **F1**, **F2** and **F3**, towards Al^{3+} *via* single (black bars) and dual (red bars) metal competitive analysis, were carried out, which demonstrated that only Al^{3+} exhibited the selective sensitivity among the 23 available metal ions (Li^+, Ag^+, K^+, Na^+, Cs^+, Ni^{2+}, Fe^{2+}, Co^{2+}, Zn^{2+}, Cd^{2+}, Pb^{2+}, In^{3+}, Ga^{3+}, Mg^{2+}, Cu^{2+}, Cr^{3+}, Fe^{3+}, Ag^{2+}, Mn^{2+}, Eu^{3+}, Hg^{2+}, Mg^{2+} and Al^{3+} in H_2O). All metal ion concentrations were kept as 60 μM in H_2O for single metal competitive analysis, whereas for dual-metal systems 60 μM of Al^{3+} + 60 μM of other metal ions in H_2O and 60 μM of Al^{3+} + 60 μM of metal ion mixtures in H_2O were taken. During the dual metal analysis, the Al^{3+} effect at 120 μM was taken and we found that an excess addition of Al^{3+} showed a small increase in the fluorescence intensity as noticed in Fig. 8. Similarly, the selective sensor responses of **F1**, **F2** and **F3** in CH_3CN/H_2O (6/4; vol/vol) to Al^{3+} ions in the presence of other interfering metal ions were evidenced in Fig. 8, and it was also noticed that the presence of Zn^{2+} did not affect their sensitivities. Furthermore, the PL intensities were found to be increased to several folds in the cases of **F2** and **F3** with greater selectivities to Al^{3+} in contrast to Zn^{2+} ions. The selectivities towards Al^{3+} rather than Zn^{2+} were explained further by ratiometric displacements and competitive binding studies later on. Similar to fluorescence titrations, UV-Vis titrations (Fig. S16, see the ESI†) also confirmed the sensitivities of **F1**, **F2** and **F3** in CH_3CN/H_2O

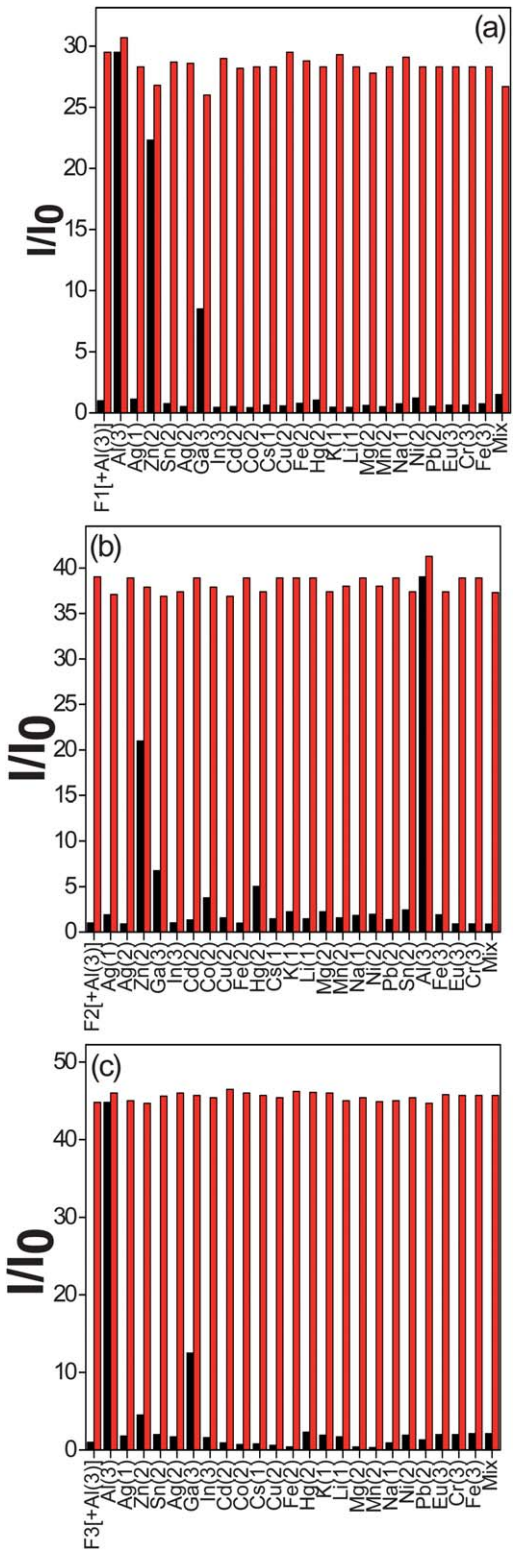

Fig. 8 Relative fluorescence intensities of (a) **F1** (20 μM), (b) **F2** (20 μM) and (c) **F3** (20 μM) in CH_3CN/H_2O (6/4; vol/vol) with 60 μM Al^{3+} in H_2O in the presence of competing metal ions. Black bars; **F1**, **F2** and **F3** (20 μM) in CH_3CN/H_2O (6/4; vol/vol) with 60 μM of stated metal ions in H_2O. Red bars; **F1**, **F2** and **F3** (20 μM) CH_3CN/H_2O (6/4; vol/vol) with 60 μM Al^{3+} + 60 μM of stated metal ions in H_2O (120 μM of Al^{3+} for Al^{3+} effect) (mix = combinations of all metal ions except Zn^{2+} and Al^{3+}).

(6/4; vol/vol) to Al^{3+} with quenching the absorption maxima at 344, 346 and 343 nm, respectively. Upon the addition of 0–40 μM Al^{3+} (0, 2, 5, 10, 15, 20, 22, 24, 28, 32, 36 and 40 μM) absorption maxima of **F1**, **F2** and **F3** were quenched rapidly up to 20 μM and thereafter found to reversible to their original states. Since **F1**, **F2** and **F3** in CH_3CN/H_2O (3/7; vol/vol) also exhibited the selectivities to Al^{3+} ions, the fluorescence titrations were performed further and our observations suggested that their sensing capabilities were not affected any more. Even though the PL intensities of **F1**, **F2** and **F3** in CH_3CN/H_2O (3/7; vol/vol) were affected little, they reproduced the almost similar fluorescence spectral responses in the presence of interfering metal ions as represented by Fig. S17–S19 (ESI†). In addition, the PL sensor responses of **F1**, **F2** and **F3** in CH_3CN/H_2O (6/4; vol/vol) were not enhanced after 5 equivalents (see Fig. S53; ESI†).

UV-Vis/PL titrations on OH^- ions

Upon the addition of OH^- 0–50 equiv., with an equal span of 5 equiv. in the form of tetrabutyl ammonium salt in H_2O, **F1**, **F2** and **F3** in CH_3CN/H_2O (6/4; vol/vol) showed the fluorescence turn-on responses *via* phenoxide ion formation as depicted in Fig. S20 (see the ESI†), and also visualized green fluorescence phenomena under UV-light irradiations (Fig. 4). The specific selectivities of **F1**, **F2** and **F3** to OH^- ions were evaluated *via* single (black bars) and dual-anion (white bars) titrations as noticed in Fig. S21 (see the ESI†). Both systems confirmed sensitivities of **F1**, **F2** and **F3** to OH^- ions in H_2O. Nevertheless, while the titrations were repeated with **F1**, **F2** and **F3** in CH_3CN/H_2O (3/7; vol/vol), we found the fewer folds of PL enhancements (Fig. S19c; see the ESI†). Since, the OH^- sensors also revealed the PL peaks roughly at *ca.* 500 nm, except the presence of Zn^{2+} and Al^{3+}, we found none of the other metal ions interfered in the sensory system. However, due to the requirement of 50 equiv. of OH^- ions, the reverse phenomena of interference of OH^- ions in Zn^{2+} or Al^{3+} sensors were not observed. But, because of the pH changes arising from inorganic metal ion hydroxide salts both Zn^{2+} and Al^{3+} sensors were found to be affected. On the other hand, UV-Vis spectra (Fig. S22a–c; see the ESI†) of **F1**, **F2** and **F3** in CH_3CN/H_2O (6/4; vol/vol) towards OH^- ions in H_2O showed the quenching effect. **F1**, **F2** and **F3** in CH_3CN/H_2O (3/7; vol/vol), exhibited barely 5.3, 4.5 and 4.7 folds of PL enhancements, respectively, which was negligible in contrast to **F1**, **F2** and **F3** in CH_3CN/H_2O (6/4; vol/vol). Hence, the OH^- sensor systems in CH_3CN/H_2O (3/7; vol/vol) were not considered further.

Stoichiometries[24] of sensor complexes

To ensure the sensor responses of **F1**, **F2** and **F3**, the stoichiometries of **F1**+Zn^{2+}, **F2**+Zn^{2+}, **F1**+Al^{3+}, **F2**+Al^{3+} and **F3**+Al^{3+} were calculated through job's plots as noticed in Fig. S23 (see the ESI†). Regarding **F1**+Zn^{2+} and **F2**+Zn^{2+}, the stoichiometric calculations were carried out based on their normalized PL intensity changes (see the insets of Fig. 5a and b), in which an excess addition of Zn^{2+} slightly affected the sensory systems. The job's plots between mole fraction (X_M) and normalized PL intensity changes of **F1**+Zn^{2+} and **F2**+Zn^{2+} went through

maxima at molar fractions of *ca.* 0.506 (**F1**+Zn^{2+}) and 0.503 (**F2**+Zn^{2+}) as shown in Fig. S23a and b (see the ESI†), respectively, indicating their 1 : 1 stoichiometric complexes. In a similar manner, the stoichiometries of **F1**+Al^{3+}, **F2**+Al^{3+} and **F3**+Al^{3+} were established by job's plots between X_M and absorption maximum changes at 344, 346 and 343 nm, respectively. Upon the addition of 0–40 μM Al^{3+} (0, 2, 5, 10, 15, 20, 22, 24, 28, 32, 36 and 40 μM), the absorption maxima of **F1**, **F2** and **F3** were quenched rapidly up to 20 μM, afterward they were found to be restored again. Therefore, the job's plots were plotted between X_M and absorption changes at 344 nm (**F1**+Al^{3+}), 346 nm (**F2**+Al^{3+}), 343 nm (**F3**+Al^{3+}), where they went through maxima at molar fractions of *ca.* 0.5 (**F1**+Al^{3+}), 0.507 (**F2**+Al^{3+}) and 0.508 (**F2**+Al^{3+}), respectively, as shown in Fig. S23c–e (see the ESI†), representing their 1 : 1 stoichiometry.

^{1}H and ^{13}C NMR titrations on sensor complexes

The sensor properties of **F1**, **F2** and **F3** were further confirmed by their binding site analysis *via* ^{1}H and ^{13}C NMR titrations.[25] For both experiments, the Zn^{2+} and Al^{3+} ions were dissolved in D_2O as well as tetrabutyl ammonium hydroxide (TBAOH) in D_2O, and titrated with **F1**, **F2** and **F3** in CD_3CN. As publicized in Fig. 9a–c, the remaining proton environments present in **F1**, **F2** and **F3** were related to the addition of Zn^{2+}, Al^{3+}, and OH^- ions, which induced the disappearance of the phenolic –OH (H_a) signal utterly. However, the ^{1}H NMR spectra of OH^- sensors were discriminated from Zn^{2+} and Al^{3+} sensors *via* the entire disappearance of the phenolic –OH (H_a) without affecting the lingering proton environment. The above observation also well supported the phenoxide ion formation in the OH^- sensor responses, but to clarify our suspicion, the mass spectral studies were also accomplished subsequently. On the other hand, upon the addition of Zn^{2+} and Al^{3+} ions in D_2O to **F1**, **F2** and **F3** in CD_3CN the phenolic –OH (H_a) totally disappears with downfield and upfield shifting of residual imine (H_b) and pyridyl (H_c) protons of **F1**, **F2** and **F3** as follows: The downfield shifting of imine (H_b) protons of **F1** (9.49 ppm), **F2** (9.45 ppm) and **F3** (9.15 ppm) were evidenced for **F1**+Zn^{2+} (9.97 ppm), **F1**+Al^{3+} (10.09 ppm), **F2**+Zn^{2+} (9.95 ppm), **F2**+Al^{3+} (10.05 ppm) and **F3**+Al^{3+} (10.05 ppm). In a similar manner, the pyridyl (H_c) protons of **F1** (8.57 ppm), **F2** (8.38 ppm) and **F3** (8.03 ppm) were downfield shifted for **F1**+Zn^{2+} (9.12 ppm), **F2**+Zn^{2+} (8.93 ppm) and **F3**+Al^{3+} (8.23 ppm) but upfield shifted for **F1**+Al^{3+} (8.12 ppm) and **F2**+Al^{3+} (7.96 ppm). Due to the higher selectivity and CHEF mechanism to Al^{3+}, **F3** provides a different NMR spectrum compared with **F1** and **F2**. Hence, the ^{1}H NMR titrations confirmed the deprotonation mechanism as well as the involvements of hetero atoms (O, N) towards sensor responses *via* ICT and CHEF. In addition, the ^{1}H NMR spectral titrations of **F1**, **F2** and **F3** with Ga^{3+} for the comparative purpose were also provided as noticed in Fig. S52 (ESI†). To re-evaluate ^{1}H NMR results, the ^{13}C NMR titrations were carried out in similar conditions and supported the involvement of hetero atoms in Zn^{2+} and Al^{3+} sensors, as well as the phenoxide formations through deprotonation of **F1**, **F2** and **F3** for OH^- sensors as shown in Fig. S24–S31 (see the ESI†). The imine group attached

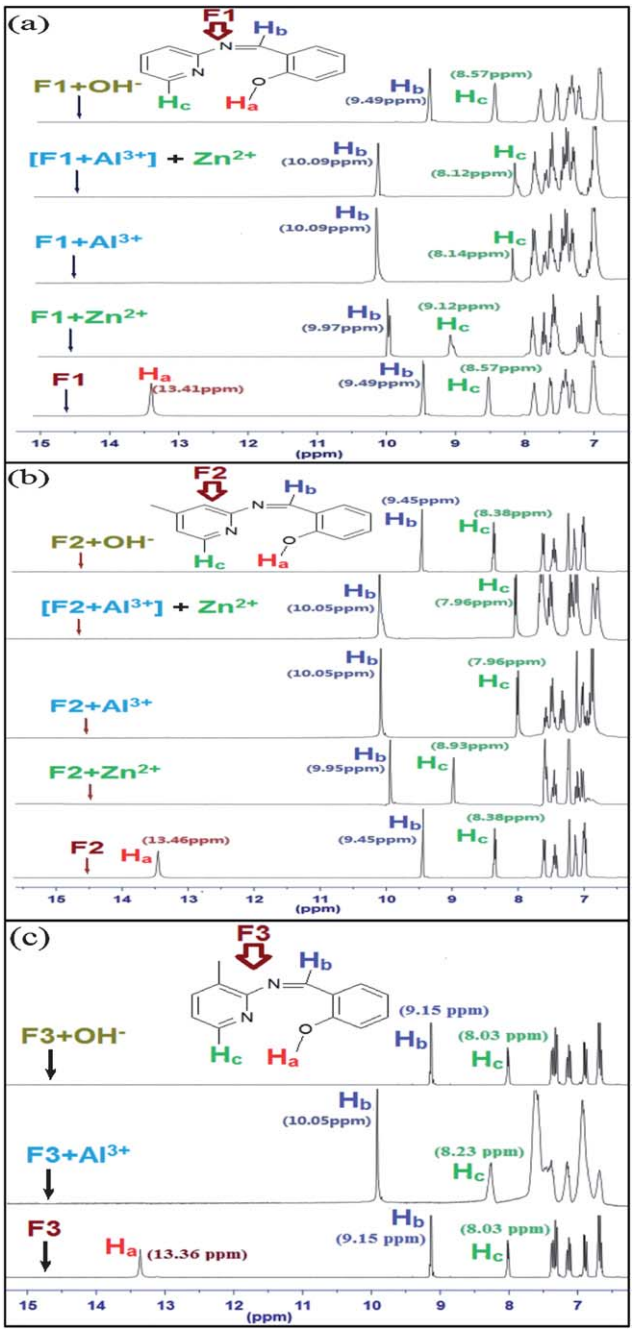

Fig. 9 ^{1}H NMR spectral changes of (a) **F1** (1 equiv.) in CD_3CN (b) **F2** (1 equiv.) in CD_3CN with Zn^{2+} (1 equiv.), Al^{3+} (1 equiv.), (Al^{3+}+Zn^{2+}) [(1 : 1) (each 3 equiv.)] and OH^- (5 equiv.) ions in D_2O, (c) **F3** (1 equiv.) in CD_3CN with Al^{3+} (1 equiv.), and OH^- (5 equiv.) ions in D_2O.

to pyridyl carbons and the –OH group attached to phenyl carbons of **F1** (162.6 and 166.0 ppm), **F2** (162.6 and 165.8 ppm) and **F3** (162.7 and 165.0 ppm) were downfield shifted for **F1**+Zn^{2+} (197.4 and 179.7 ppm) and **F2**+Zn^{2+} (197.4 and 179.9 ppm), respectively. However, in the case of **F1**+Al^{3+} (198.0 and 165.9 ppm), **F2**+Al^{3+} (198.0 and 165.7 ppm) and **F3**+Al^{3+} (197.4 and 165.7 ppm), the –OH group attached to phenyl carbons had less downfield shifts in comparison with their individual zinc complexes, and hence ^{13}C NMR spectra became distinguishable. As found in ^{1}H NMR, **F3**+Al^{3+} did not evidence the

different spectrum in contrast to **F1**+Al^{3+} and **F2**+Al^{3+}, this might be because of similar binding site. Even though residual carbon atoms of **F1**, **F2** and **F3** showed some downfield and upfield shifts, we explained the main affected carbons for simplicity, and both ^{1}H and ^{13}C NMR titrations ensured the stoichiometries of sensor complexes. Due to the high concentration requirements of NMR measurements, ^{13}C NMR titrations of **F1**, **F2** and **F3** did not show noticeable changes towards Ga^{3+}, so these related spectra are not presented.

Mass (FAB) spectra[26] of sensor complexes

The mass spectra of sensor complexes confirmed the binding sites and phenoxides formation along with the stoichiometries as noticed in Fig. S32–S39 (see the ESI†). The phenoxide formations during the OH^- sensor responses were evidenced by their respective mass peaks [$m/z = 197$ (**F1**-phnoxide) and $m/z = 211$ (**F2** and **F3**-phenoxides)] in conjunction with intense TBAOH peaks (Fig. S37–S39; see the ESI†). In the same way, mass spectra of **F1**+Zn^{2+} ($m/z = 259$), **F2**+Zn^{2+} ($m/z = 273$), **F1**+Al^{3+} ($m/z = 221$), **F2**+Al^{3+} ($m/z = 235$) and **F3**+Al^{3+} ($m/z = 235$) clearly indicated the participation of hetero atoms (O, N) and stoichiometries of the above sensor materials (Fig. S32–S36†). Apart from the peaks of sensor metal complexes, we also found the primitive peaks of **F1**, **F2** and **F3** along with their metal ion sources, due to the presence of simple equilibria. In addition to the mass spectra of **F1**+Zn^{2+} and **F2**+Zn^{2+}, their binding sites were further inveterated by the reversibilities of the sensor complexes[27] as revealed in Fig. S40 (see the ESI†). While adding 1 equiv. of EDTA to **F1**+Zn^{2+} and **F2**+Zn^{2+}, they were found to be reversible to their original state (**F1** and **F2**). Further investigation also proved that both of them could act as reusable sensor materials up to 10 cycles (Fig. S40e and f†). Hence, the binding sites, stoichiometries, and phenoxide ion formations were well recognized through mass spectral studies.

Detection limits (LODs)[28] of sensor complexes

In order to prove the selectivities of **F1**, **F2** and **F3** towards discernible detections of Zn^{2+}, Al^{3+}, and OH^- ions, the calculations of detection limits (LODs) were performed through standard deviations and linear fittings as shown in Fig. S41 and S42 (see the ESI†) by plotting the relative fluorescence intensity (I/I_0) changes as a function of concentration. The detection limits were evidenced as 4.22×10^{-7}, 4.89×10^{-7}, 1.69×10^{-6}, 1.42×10^{-6} and 1.27×10^{-6} M, for **F1**+Zn^{2+}, **F2**+Zn^{2+}, **F1**+Al^{3+}, **F2**+Al^{3+} and **F3**+Al^{3+} complexes, respectively. In contrast to Al^{3+}, the LODs of Ga^{3+} were found to be 10^{-6} levels (Fig. S54, ESI†), but no conceivable sensor responses were observed with higher concentrations of Ga^{3+} (Fig. S53, ESI†). Similarly, the LODs of **F1**+OH^-, **F2**+OH^- and **F3**+OH^- were estimated as 2.79×10^{-5}, 2.89×10^{-5} and 2.78×10^{-5} M, respectively, and confirmed that they were in an affordable range.

Ratiometric displacements[29] of Zn^{2+}

Fig. 10 supported the ratiometric fluorescence intensity changes during the addition of Al^{3+} solution to **F1**+Zn^{2+} ($\lambda_{em} = 508$ nm) or **F2**+Zn^{2+} ($\lambda_{em} = 505$ nm), in which the ratiometric displacements of Zn^{2+} by Al^{3+} were noticed. While adding 0–80 μM Al^{3+} to **F1**+Zn^{2+} and **F2**+Zn^{2+} in the previous processes, both showed PL quenching up to 20 μM, peaks of **F1**+Al^{3+} ($\lambda_{em} = 487$ nm) and **F2**+Al^{3+} ($\lambda_{em} = 485$ nm) appeared. In addition, the above ratiometric displacements were well verified by ^{1}H, ^{13}C NMR, mass, and TRPL studies, which were entirely matched with **F1**+Al^{3+} and **F2**+Al^{3+} complexes. In ^{1}H NMR spectra (Fig. 9a and b), the imine (H_b) and pyridyl (H_c) protons of [**F1**+Al^{3+}] + Zn^{2+} (10.09 and 8.12 ppm) and [**F2**+Al^{3+}] + Zn^{2+} (10.05 and 7.96 ppm) were totally in line with the imine (H_b) and pyridyl (H_c) protons of **F1**+Al^{3+} (10.09 and 8.14 ppm) and **F2**+Al^{3+} (10.05 and 7.96 ppm). Furthermore, as publicized in ^{13}C NMR spectra (Fig. S43 and S44; see the ESI†) the imine group attached to pyridyl carbons and the –OH group attached to phenyl carbons of [**F1**+Al^{3+}] + Zn^{2+} (197.8 and 165.9 ppm, respectively) and [**F2**+Al^{3+}] + Zn^{2+} (197.8 and 165.7 ppm, respectively) were similar to **F1**+Al^{3+} (198.0 and 165.9 ppm, respectively) and **F2**+Al^{3+} (198.0 and 165.7 ppm, respectively), which confirmed the ratiometric displacements of Zn^{2+} by Al^{3+} in **F1**+Zn^{2+} and **F2**+Zn^{2+} complexes. In addition to ^{1}H and ^{13}C NMR spectral studies, mass spectra (Fig. S45 and S46; see the ESI†) of [**F1**+Al^{3+}] + Zn^{2+} and [**F2**+Al^{3+}] + Zn^{2+} provided the m/z intense peaks of **F1**+Al^{3+} ($m/z = 221$) and **F2**+Al^{3+} ($m/z = 235$) along with the little intense peaks of **F1**+Zn^{2+} ($m/z = 259$), **F2**+Zn^{2+} ($m/z = 273$). The

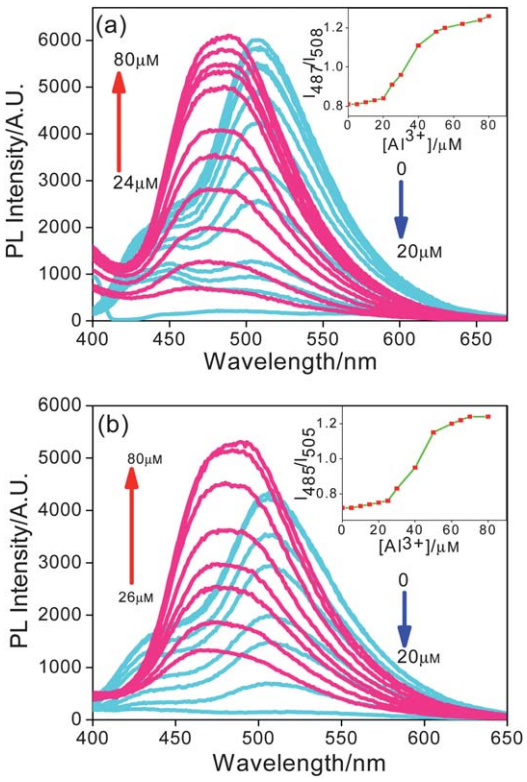

Fig. 10 Fluorescence spectra of (a) [**F1**+Zn^{2+}] (20 μM **F1** in CH_3CN/H_2O (6/4; vol/vol) mixed with 20 μM Zn^{2+} in H_2O), and (b) [**F2**+Zn^{2+}] (20 μM **F2** in CH_3CN/H_2O (6/4; vol/vol) mixed with 20 μM Zn^{2+} in H_2O) upon the addition of Al^{3+} in H_2O (0, 2, 8, 12, 14, 16.18, 20, 24, 30, 38, 48, 56, 62, 68, 76 and 80 μM and 0, 2, 8, 12, 14, 16.18, 20, 26, 32, 38, 48, 56, 62, 68, 76 and 80 μM, respectively). Inset: ratiometric fluorescence intensity [I_{487}/I_{508}] and [I_{485}/I_{505}] as a function of [Al^{3+}].

above observations verified the ratiometric displacements and the simple equilibrium present in the system. Apart from the PL, ^{1}H, ^{13}C NMR, and mass studies, the decay constant (τ) values of [**F1**+Al^{3+}] + Zn^{2+} and [**F2**+Al^{3+}] + Zn^{2+} derived from TRPL spectra in Fig. S48c–f† also coincided with **F1**+Al^{3+} and **F2**+Al^{3+} as shown in Tables S1 and S2 (see the ESI†), which was further explained in the end (TRPL spectra of sensor complexes). As shown in Fig. 10, the displacements of Zn^{2+} by Al^{3+} was evidenced through their differential spectral shifts arising from the ICT mechanism.

Competitive binding analysis

To evaluate the higher binding ability of Al^{3+} ions compared with Zn^{2+} ions, the competitive binding analyses were utilized as reported in the literature.[30] Regarding Zn^{2+} and Al^{3+} the association constants (log K_a) were calculated by plotting response parameter values (α) as a function of logarithm [Zn^{2+}] and [Al^{3+}] based on $[Zn^{2+}] = 1/2K_aL(1 - \alpha/\alpha^2)$ and $[Al^{3+}] = 1/3K_aL^2(1 - \alpha/\alpha^3)$; where L was the ligand and α was defined as a ratio between the free ligand concentration [L] and the initial ligand concentration [L_0]. As evidenced in Fig. S47 (see the ESI†), the plots between response parameter values (α) and [Zn^{2+}] or [Al^{3+}] for **F1**, **F2** and **F3** revealed the association constants (log K_a) of Zn^{2+} and Al^{3+} complexed as **F1**+Zn^{2+}, **F2**+Zn^{2+}, **F1**+Al^{3+}, **F2**+Al^{3+} and **F3**+Al^{3+} sensor materials. The log K_a values of Zn^{2+} in **F1**+Zn^{2+} and **F2**+Zn^{2+} were identified as 7.92 and 7.76, respectively, whereas it was found to be larger for Al^{3+} in **F1**+Al^{3+}, **F2**+Al^{3+} and **F3**+Al^{3+} (10.96, 11.64 and 12.38, respectively). Higher log K_a values of Al^{3+} ions rather than Zn^{2+} ions well supported the ratiometric displacements of Zn^{2+} by Al^{3+} in **F1**+Zn^{2+} and **F2**+Zn^{2+} along with the greater selectivity of **F1**, **F2** and **F3** to Al^{3+} ions in contrast to Zn^{2+} ions. Furthermore, at higher concentrations of Ga^{3+} ions (5–10 equiv.) the sensor responses were not enhanced as in the case of Al^{3+} ions, therefore the association constant calculations for Ga^{3+} ions were not provided. Furthermore, the log K_a values (Table S1†) also supported the decay constant (τ) values obtained from the time resolved photoluminescence spectra of sensor complexes (**F1**+Zn^{2+}, **F2**+Zn^{2+}, **F1**+Al^{3+}, **F2**+Al^{3+} and **F3**+Al^{3+}).

TRPL spectra and quantum yields (Φ) of sensor complexes

As reported in the literature[31] and from our results (Fig. S48a–j†), we found that the fluorescence decay constants (τ) were affected typically by turn-on sensor responses as summarized in Table 1, S1 and S2 (see the ESI†). From the TRPL signals without any sensor responses the fluorescence life time values of **F1**, **F2** and **F3** were 2.19, 1.51, and 1.35 ns, respectively. During the **F1**+Zn^{2+} and **F2**+Zn^{2+} sensing processes, the faster decay components (A_1) of **F1** and **F2** (89.2% and 95.1%) were decreased to 27.5% and 27.6%, respectively, along with increased values of longer decay components (A_2) as shown in Table S2.† Similar trends were evidenced in **F1**+Al^{3+}, **F2**+Al^{3+}, **F3**+Al^{3+}, **F1**+OH^-, **F2**+OH^- and **F3**+OH^- sensing responses, and their ultrafast decay time constant (τ_1) values and longer decay time constant (τ_2) values were affected rapidly according to the results of biexponential decay fittings. Except **F1**+Al^{3+}, **F2**+Al^{3+}, and **F3**+Al^{3+} sensors, the other sensors (**F1**+Zn^{2+}, **F2**+Zn^{2+}, **F1**+OH^-, **F2**+OH^- and **F3**+OH^-) have smaller τ_1 and higher τ_2 values, whereas in the previous cases (Al^{3+} complexes) those values were in the reverse tendency. Based on single exponential decay fittings, the average fluorescence life time values of **F1**+Zn^{2+}, **F2**+Zn^{2+}, **F1**+Al^{3+}, **F2**+Al^{3+}, **F3**+Al^{3+}, **F1**+OH^-, **F2**+OH^- and **F3**+OH^- were estimated as 4.15, 3.83, 11.97, 11.53, 12.16, 3.95, 2.28 and 2.18 ns, respectively. In addition to the above sensory systems, the [**F1**+Al^{3+}] + Zn^{2+} and [**F2**+Al^{3+}] + Zn^{2+} sensor materials were also shown in Fig. S48f and g,† in which both of them reproduced the similar TRPL properties (Table S2†) of **F1**+Al^{3+} and **F2**+Al^{3+}. Hence, TRPL properties supported the ratiometric displacement behavior of Zn^{2+} by Al^{3+} in **F1**+Zn^{2+} and **F2**+Zn^{2+} and also confirmed the higher binding ability of Al^{3+} ions. In general, the greater fluorescence life time (τ_{Avg}) values of **F1**+Al^{3+}, **F2**+Al^{3+}, and **F3**+Al^{3+} (11.97, 11.53, and 12.16 ns, respectively) sensor materials established better Al^{3+} selectivities of **F1**, **F2** and **F3**. Similarly, the modest sensor responses of **F1**+Al^{3+}, **F2**+Al^{3+}, and **F3**+Al^{3+} were evidenced by their decay constants as noticed in Tables S1 and S2.† In addition, the negligible selectivities of **F1**, **F2** and **F3** towards Ga^{3+} were confirmed by their TRPL results (Fig. S55, ESI†). Furthermore, the quantum yield (Φ) values[32] of **F1**+Zn^{2+}, **F2**+Zn^{2+}, **F1**+Al^{3+}, **F2**+Al^{3+}, **F3**+Al^{3+}, **F1**+OH^-, **F2**+OH^- and **F3**+OH^- sensor complexes reconfirmed the sensitivities of **F1**, **F2** and **F3**. For **F1**+Zn^{2+} and **F2**+Zn^{2+} sensors, the Φ values of **F1** and **F2** (0.011 and 0.008) were enhanced 25.5 and 24.5 times, respectively, as shown in Table S1.† Similarly, **F1**+Al^{3+}, **F2**+Al^{3+}, **F3**+Al^{3+}, **F1**+OH^-, **F2**+OH^- and **F3**+OH^- sensor complexes demonstrated 26.4, 27.6, 30.7, 20.0, 15.2 and 17.1 times higher Φ values than their respective probes **F1**, **F2** and **F3** (0.011, 0.008, and 0.01). More interestingly, the Φ values of [**F1**+Al^{3+}] + Zn^{2+} and [**F2**+Al^{3+}] + Zn^{2+} were similar to those of **F1**+Al^{3+} and **F2**+Al^{3+}, and verified the higher selectivities towards Al^{3+} ions. The Φ values of **F1**+Ga^{3+}, **F2**+Ga^{3+} and **F3**+Ga^{3+} are also noticed for their modest sensor responses provided by Ga^{3+} (see Table S1†).

Time and temperature effects[33]

In general, sensor recognitions are time dependent and in many cases they were rapid, but in some cases they were found to be time consuming. Therefore, the above mentioned sensor complex (**F1**+Zn^{2+}, **F2**+Zn^{2+}, **F3**+Zn^{2+}, **F1**+Al^{3+}, **F2**+Al^{3+}, **F3**+Al^{3+}, **F1**+OH^-, **F2**+OH^- and **F3**+OH^-) recognitions were evaluated with respect to time in seconds as shown in Fig. 11a and b. The Zn^{2+} or Al^{3+} ions in H_2O were added to **F1**, **F2** and **F3** in CH_3CN/H_2O (6/4; vol/vol) as per the stoichiometry (1 : 1), and the PL intensity changes were analyzed as a function of time/seconds. As envisioned in Fig. 11a, the sensor recognitions of Zn^{2+} were rapid within 20 seconds, thereafter the intensity remains identical. On the other hand, the PL intensities to sensor detections of Al^{3+} ions were slowly amplified with respect to time (0–180 seconds), as represented by Fig. 11b. In the same way, upon the direct addition of 50 equiv. of TBAOH to **F1**, **F2** and **F3**, the PL intensity of OH^- sensor responses were quick (20 seconds) as noted in Fig. 11c. In addition to the individual sensor responses, we also checked the ratiometric sensor

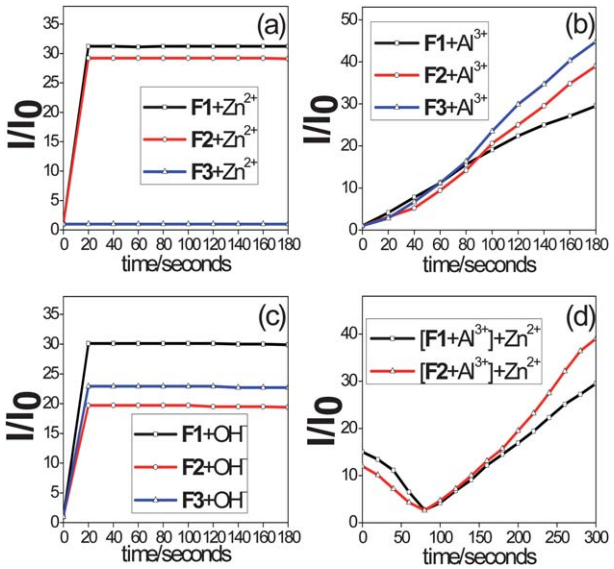

Fig. 11 PL spectral responses of (a) **F1**+Zn^{2+}, **F2**+Zn^{2+} and **F3**+Zn^{2+} (1 : 1), (b) **F1**+Al^{3+}, **F2**+Al^{3+} and **F3**+Al^{3+} (1 : 1), (c) **F1**+OH^-, **F2**+OH^- and **F3**+OH^- (1 : 50), and (d) [**F1**+Al^{3+}] + Zn^{2+} and [**F2**+Al^{3+}] + Zn^{2+} (1 : 1 : 1), as a function of time (seconds).

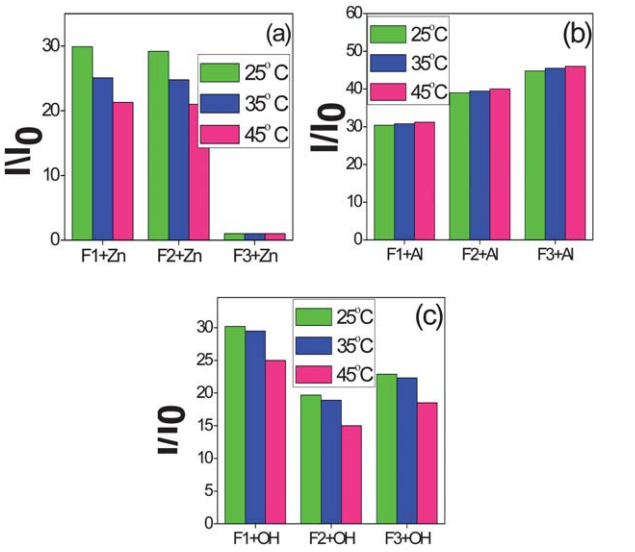

Fig. 12 PL spectral responses of (a) **F1**+Zn^{2+}, **F2**+Zn^{2+} and **F3**+Zn^{2+}, (b) **F1**+Al^{3+}, **F2**+Al^{3+} and **F3**+Al^{3+}, and (c) **F1**+OH^-, **F2**+OH^- and **F3**+OH^-, as a function of temperature (25, 35 and 45 °C).

responses of **F1**+Zn^{2+} and **F2**+Zn^{2+} by Al^{3+} as a function of time/seconds. Fig. 11d verified the greater selectivity of Al^{3+} with regard to time (0–300 seconds) in ratiometric displacements of Zn^{2+} (**F1**+Zn^{2+} and **F2**+Zn^{2+}). After the recognition process, we further extended time effects (0–60 minutes) to **F1**+Zn^{2+}, **F2**+Zn^{2+}, **F1**+Al^{3+}, **F2**+Al^{3+}, **F3**+Al^{3+}, **F1**+OH^-, **F2**+OH^- and **F3**+OH^- sensor complexes, as shown in Fig. S49 (see the ESI†). After the sensor detection processes, except the Al^{3+} sensors (Fig. S49b†), none of the above sensor responses provided the incredible PL intensity changes up to 1 hour. Owing to the importance of temperature in the sensor responses, we checked the sensitivities of **F1**, **F2** and **F3** in CH_3CN/H_2O (6/4; vol/vol) to Zn^{2+}, Al^{3+} and OH^- ions at three different temperatures like 25, 35, and 45 °C. As revealed in Fig. 12a and c, upon increasing the temperature (25–45 °C) the sensor responses towards Zn^{2+} and OH^- showed the decreasing trend. However, Al^{3+} sensor responses (Fig. 12b) were increased regarding temperature increment, and hence confirmed the higher selectivities towards Al^{3+}.

Solvent concentration and pH effects

To evaluate our decision to use the CH_3CN/H_2O (6/4 and 3/7; vol/vol) aqueous media for sensor titrations, the solvent effects[34] on the PL intensities of sensor responses were performed by increasing the H_2O amount (0–99%), as exposed in Fig. S50 (see the ESI†). The PL intensities of probes **F1**, **F2** and **F3** (Fig. S50a†) were not affected incredibly up to 40% of H_2O and thereafter showed a little effect up to 70% of H_2O but affected further again within 70–99% of H_2O. At the same time, the sensor PL intensities of **F1** and **F2** in CH_3CN (Fig. S50b†) to Zn^{2+} were completely quenched while increasing the portion of H_2O more than 50%, but the PL intensities of sensor responses of **F1**, **F2** and **F3** in CH_3CN (Fig. S50c†) to Al^{3+} remained identical up to 70% of H_2O. However, even at higher proportions of H_2O (80–99%), they illustrated the sensor selectivities towards Al^{3+} to some folds roughly around *ca.* 10, 7, and 5 folds (80, 90, and 99%, respectively). The above observations also confirmed that, at higher H_2O proportion (>50%), the ICT and *cis–trans* interconversion were restricted, and provided selectivities just to Al^{3+} *via* CHEF. On the other hand, the PL intensities of OH^- sensors of **F1**, **F2** and **F3** in CH_3CN (Fig. S50d†) remained similar up to 50% of H_2O, but later on they were rapidly quenched. In general, Fig. S50† verified that **F1**, **F2** and **F3** provided the higher selectivities towards Al^{3+} with negligible selectivities to OH^- at 80–99% semi-aqueous media.

Since previous reports[35] have noted the necessity of effective pH for the sensor responses, we tend to analyze our sensor systems with various pHs (0–14) as shown in Fig. S10 (see the ESI†). The PL intensities of **F1**, **F2** and **F3** in CH_3CN/H_2O (6/4; vol/vol) were little quenched at acidic pHs (0–5) and show highly intense peaks at basic pHs (9–14) due to the stable phenoxide formations as noticed in Fig. S11.† Further investigations of fluorescence spectra of **F1**, **F2** and **F3** in CH_3CN/H_2O (6/4; vol/vol) at pH = 12 provided intense PL peaks at 525, 527, and 512 nm, respectively, which might arise from their phenoxides as in the case of OH^- sensors. Moreover, the TRPL decay constant (τ_{Avg}) values were decreased for acidic pHs and increased for the basic pHs as summarized in Table S2,† and hence confirmed that they can be also used as pH sensors to differentiate acidic and basic pHs. Fig. S12† illustrated the TRPL spectra of **F1**, **F2** and **F3** in CH_3CN/H_2O (6/4; vol/vol) and the inset shows the photographs of acidic, neutral, and basic pHs (2, 7, and 12) under UV-light irradiations, where the green fluorescence was due to phenoxide formations at pH = 12. Further analysis of pH effects on the sensor responses were exposed in Fig. S51a–c (see the ESI†), in which **F1**, **F2** and **F3** in CH_3CN/H_2O (6/4 and 3/7; vol/vol) towards both Zn^{2+} and Al^{3+} sensors were affected rapidly

at acidic and basic pHs (0–5 and 9–14), but have no effects between 6 and 8 pHs. At the same time, the PL intensities of OH^- sensor responses of **F1**, **F2** and **F3** in CH_3CN/H_2O (6/4; vol/vol) were rapidly affected at acidic pHs (0–5), and have no effect at neutral and basic pHs (6–14). In other words, the OH^- sensor responses at basic pHs were even better due to the increased stabilities of phenoxides. Therefore, from the pH effect studies we concluded that sensor responses of **F1**, **F2** and **F3** towards Zn^{2+} and Al^{3+} were effective between 6 and 8 pHs, and OH^- sensors were effective between 6 and 14 pHs.

Conclusions

In conclusion, three pyridyl-salicylimine derivatives (**F1**, **F2** and **F3**) were easily synthesized *via* one-step aldamine condensation, and utilized for the first time as fluorescence "turn-on" sensors for distinct detections of Zn^{2+}, Al^{3+} and OH^- ions in mixed-aqueous media [CH_3CN/H_2O (6/4 and 3/7; vol/vol), pH = 7 and at 25 °C]. **F1** and **F2** in CH_3CN/H_2O (6/4; vol/vol) exhibited fluorescence turn-on sensor responses to Zn^{2+} and Al^{3+} with differential spectral shifts, but **F3** in CH_3CN/H_2O (6/4; vol/vol) showed turn-on sensing only to Al^{3+} ions *via* ICT and CHEF. In addition, all of them (**F1**, **F2** and **F3**) in CH_3CN/H_2O (6/4) revealed the turn-on sensor responses to OH^- ions through phenoxide ion formations. Furthermore, **F1**+Zn^{2+} and **F2**+Zn^{2+} sensor complexes in CH_3CN/H_2O (6/4) evidenced the reversibilities and ratiometric displacements of Zn^{2+} with EDTA and Al^{3+} ions, respectively. The 1 : 1 stoichiometries of sensor complexes (**F1**+Zn^{2+}, **F2**+Zn^{2+}, **F1**+Al^{3+}, **F2**+Al^{3+} and **F3**+Al^{3+}) were identified from job's plots based on UV/Vis and PL spectral changes. Binding sites of sensor complexes, involvements of hetero atoms (O, N) in sensor recognitions *via* ICT, CHEF, deprotonation of phenolic –OH, and phenoxide formations were well established by ^1H, ^{13}C NMR, and mass (FAB) spectral studies. The typical detection limits (LODs) of **F1**+Zn^{2+}, **F2**+Zn^{2+}, **F1**+Al^{3+}, **F2**+Al^{3+} and **F3**+Al^{3+} sensor complexes were calculated as 4.22×10^{-7}, 4.89×10^{-7}, 1.69×10^{-6}, 1.42×10^{-6}, and 1.27×10^{-6} M, respectively, by standard deviations and linear fittings. Similarly, the LODs of **F1**+OH^-, **F2**+OH^- and **F3**+OH^- were estimated as 2.79×10^{-5}, 2.89×10^{-5}, and 2.78×10^{-5} M, respectively. The TRPL decay constant (τ) and association constant ($\log K_a$) values confirmed the better selectivities of **F1**, **F2** and **F3** towards Al^{3+} rather than both Zn^{2+} and OH^- ions. In contrast to ion selective electrodes, these sensors can be used for cell image studies in the biological systems (which are underway) involving Zn^{2+} and Al^{3+} ions. Since ion selective electrodes are corrosive at higher pH values, **F1**, **F2** and **F3** can be utilized as selective sensors at higher concentrations of OH^- ions *via* strong green emissions under UV-light irradiations. In addition, they can also be utilized as distinct spectral detections of Zn^{2+}, Al^{3+} and OH^- ions *via* peak intensity and spectral shifts corresponding to their concentrations.

Acknowledgements

We are grateful to the National Science Council of Taiwan (ROC) through NSC99-2113-M-009-006-MY2 for the financial support. We wish to thank Mandapati V. Ramakrishnam Raju for HOMO–LUMO calculations.

Notes and references

1 (*a*) V. Amendola, L. Fabbrizzi, F. Forti, M. Licchelli, C. Mangano, P. Pallavicini, A. Poggi, D. Sacchi and A. Taglieti, *Coord. Chem. Rev.*, 2006, **250**, 273; (*b*) D. Astruc, E. Boisselier and C. Ornelas, *Chem. Rev.*, 2010, **110**, 1857; (*c*) J. Wu, W. Liu, J. Ge, H. Zhang and P. Wang, *Chem. Soc. Rev.*, 2011, **40**, 3483; (*d*) X. Chen, S. W. Nam, G. H. Kim, N. Song, Y. Jeong, I. Shin, S. K. Kim, J. Kim, S. Park and J. Yoon, *Chem. Commun.*, 2010, **46**, 8953.

2 (*a*) A. P. de Silva, H. Q. N. Gunaratne, T. Gunnlaugsson, A. J. M. Huxley, C. P. McCoy, J. T. Rademacher and T. E. Rice, *Chem. Rev.*, 1997, **97**, 1515; (*b*) A. K. Dwivedi, G. Saikia and P. K. Iyer, *J. Mater. Chem.*, 2011, **21**, 2502; (*c*) S. Sumalekshmy and C. J. Fahrni, *Chem. Mater.*, 2011, **23**, 483.

3 (*a*) N. Niamnont, R. Mungkarndee, I. Techakriengkrai, P. Rashatasakhon and M. Sukwattanasinitt, *Biosens. Bioelectron.*, 2010, **26**, 863; (*b*) X. Lou, D. Ou, Q. Li and Z. Li, *Chem. Commun.*, 2012, **48**, 8462.

4 (*a*) D. T. McQuade, A. E. Pullen and T. M. Swager, *Chem. Rev.*, 2000, **100**, 2537; (*b*) G. Aragay, J. Pons and A. Merkoci, *Chem. Rev.*, 2011, **111**, 3433.

5 (*a*) M. Sauer, *Angew. Chem., Int. Ed.*, 2003, **42**, 1790; (*b*) A. P. de Silva, T. S. Moody and G. D. Wright, *Analyst*, 2009, **134**, 2385.

6 (*a*) J. Wu, W. Liu, J. Ge, H. Zhang and P. Wang, *Chem. Soc. Rev.*, 2011, **40**, 3483; (*b*) P. Kaur, D. Sareen and K. Singh, *Dalton Trans.*, 2012, **41**, 9607; (*c*) Y. Chen, C. Zhu, Z. Yang, J. Li, Y. Chiao, W. He, J. Chen and Z. Guo, *Chem. Commun.*, 2012, **48**, 5094; (*d*) R. Satapathy, Y. S. Wu and H. C. Lin, *Org. Lett.*, 2012, **14**, 2564.

7 (*a*) D. A. Pearce, N. Jotterand, I. S. Carrico and B. Imperiali, *J. Am. Chem. Soc.*, 2001, **123**, 5160; (*b*) J. A. Zhou, X. L. Tang, J. Cheng, Z. H. Ju, L. Z. Yang, W. S. Liu, C. Y. Chena and D. C. Bai, *Dalton Trans.*, 2012, **41**, 10626; (*c*) H. Y. Lin, P. Y. Cheng, C. F. Wan and A. T. Wu, *Analyst*, 2012, **137**, 4415; (*d*) Y. Bao, B. Liu, F. Du, J. Tian, H. Wang and R. Bai, *J. Mater. Chem.*, 2012, **22**, 5291; (*e*) R. Satapathy, Y. S. Wu and H. C. Lin, *Chem. Commun.*, 2012, **48**, 5668.

8 (*a*) J. M. Berg and Y. Shi, *Science*, 1996, **271**, 1081; (*b*) X. M. Xie and T. G. Smart, *Nature*, 1991, **349**, 521.

9 (*a*) A. Torrado, G. K. Walkup and B. Imperiali, *J. Am. Chem. Soc.*, 1998, **120**, 609; (*b*) T. Jin, J. Lu and M. Nordberg, *NeuroToxicology*, 1998, **19**, 529; (*c*) V. Bhalla, Roopa and M. Kumar, *Dalton Trans.*, 2013, **42**, 975.

10 (*a*) Z. Xu, J. Yoon and D. R. Spring, *Chem. Soc. Rev.*, 2010, **39**, 1996; (*b*) Y. Xu, J. Meng, L. Meng, Y. Dong, Y. Cheng and C. Zhu, *Chem.–Eur. J.*, 2010, **16**, 12898; (*c*) X. Liu, N. Zhang, J. Zhou, T. Chang, C. Fang and D. Shangguan, *Analyst*, 2013, **138**, 901; (*d*) Y. Mikata, A. Yamashita, K. Kawata, H. Konno, S. Itami, K. Yasuda and S. Tamotsu, *Dalton Trans.*, 2012, **41**, 4976.

11 E. Delhaize and P. R. Ryan, *Plant Physiol.*, 1995, **107**, 315.

12 (*a*) G. D. Fasman, *Coord. Chem. Rev.*, 1996, **149**, 125; (*b*) Y. W. Wang, M. X. Yu, Y. H. Yu, Z. P. Bai, Z. Shen, F. Y. Li and X. Z. You, *Tetrahedron Lett.*, 2009, **50**, 6169; (*c*) S. H. Kim, H. S. Cho, J. Kim, S. J. Lee, D. T. Quang and J. S. Kim, *Org. Lett.*, 2010, **12**, 560.

13 (*a*) L. Basabe-Desmonts, D. N. Reinhoudt and M. Crego-Calama, *Chem. Soc. Rev.*, 2007, **36**, 993–1017; (*b*) M. Zhang, Y. Q. Liu and B. C. Ye, *Chem.–Eur. J.*, 2012, **18**, 2507–2513; (*c*) X. Sun, Y. W. Wang and Y. Peng, *Org. Lett.*, 2012, **14**, 3420.

14 (*a*) T. H. Ma, M. Dong, Y. M. Dong, Y. W. Wang and Y. Peng, *Chem.–Eur. J.*, 2010, **16**, 10313 and references therein; (*b*) S. Kim, J. Y. Noh, K. Y. Kim, J. H. Kim, H. K. Kang, S. W. Nam, S. H. Kim, S. Park, C. Kim and J. Kim, *Inorg. Chem.*, 2012, **51**, 3597; (*c*) S. Sen, T. Mukherjee, B. Chattopadhyay, A. Moirangthem, A. Basu, J. Marek and P. Chattopadhyay, *Analyst*, 2012, **137**, 3975; (*d*) Y. W. Liu, C. Hung Chen and A. T. Wu, *Analyst*, 2012, **137**, 5201; (*e*) S. Sinha, R. R. Koner, S. Kumar, J. Mathew, P. V. Monisha, I. Kazia and S. Ghosh, *RSC Adv.*, 2013, **3**, 345.

15 J. Du, M. Hu, J. Fan and X. Peng, *Chem. Soc. Rev.*, 2012, **41**, 4511.

16 H. Xu and O. A. Sadik, *Analyst*, 2000, **125**, 1783.

17 (*a*) R. J. Berman, G. D. Christian and L. W. Burgess, *Anal. Chem.*, 1990, **62**, 2066; (*b*) L. R. Allain and Z. Xue, *Anal. Chem.*, 2000, **72**, 1078.

18 (*a*) L. Fabbrizzi, M. Licchelli, F. Mancin, M. Pizzeghello, G. Rabaioli, A. Taglietti, P. Tecilla and U. Tonellato, *Chem.–Eur. J.*, 2002, **8**, 94; (*b*) C. Ma, A. Lo, A. Abdolmaleki and M. J. MacLachlan, *Org. Lett.*, 2004, **6**, 3841.

19 (*a*) Z. B. Li, J. Lin and L. Pu, *Angew. Chem., Int. Ed.*, 2005, **44**, 1690; (*b*) D. Maity and T. Govindaraju, *Chem.–Eur. J.*, 2011, **17**, 1410; (*c*) D. Maity and T. Govindaraju, *Inorg. Chem.*, 2011, **50**, 11282.

20 (*a*) H. Komatsu, D. Citterio, Y. Fujiwara, K. Minamihasi, Y. Araki, M. Hagiwara and K. Suzuki, *Org. Lett.*, 2005, **7**, 2857; (*b*) A. D. Cort, P. D. Bernardin, G. Forte and F. Y. Mihan, *Chem. Soc. Rev.*, 2010, **39**, 3863; (*c*) J. F. Jang, Y. Zhou, J. Yoon and J. S. Kim, *Chem. Soc. Rev.*, 2011, **40**, 3416.

21 (*a*) K. Krzysztof and I. Kuzniarska-Biernacka, *Struct. Chem.*, 2010, **21**, 357; (*b*) R. K. Dubey, P. Baranwal, S. K. Dwivedi and U. N. Tripathi, *J. Coord. Chem.*, 2011, **64**, 2649.

22 C. G. Freiherr von Richthofen, A. Stammler, H. Bogge and T. Glaser, *J. Org. Chem.*, 2012, **77**, 1435.

23 M. R. Silva-Junior and W. Thiel, *J. Chem. Theory Comput.*, 2010, **6**, 1546.

24 (*a*) S. Muthaiah, Y. C. Rajan and H. C. Lin, *J. Mater. Chem.*, 2012, **22**, 8976; (*b*) Y. C. Rajan, S. Muthaiah, C. T. Huang, H. C. Lin and H. C. Lin, *Tetrahedron*, 2012, **68**, 7926; (*c*) R. Satapathy, H. Padhy, Y. H. Wu and H. C. Lin, *Chem.–Eur. J.*, 2012, **18**, 16061; (*d*) S. Muthaiah, Y. H. Wu, A. Singh, M. V. R. Raju and H. C. Lin, *J. Mater. Chem. A*, 2013, **1**, 1310.

25 W. Zhou, Y. Li, Y. Li, H. Liu, S. Wang, C. Li, M. Yuan, X. Liu and D. Zhu, *Chem.–Asian J.*, 2006, **1–2**, 224–230.

26 (*a*) J. Yuasa and S. Fukuzumi, *J. Am. Chem. Soc.*, 2006, **128**, 15976–15977; (*b*) X. Zhou, B. Yu, Y. Guo, X. Tang, H. Zhang and W. Liu, *Inorg. Chem.*, 2010, **49**, 4002.

27 (*a*) R. Sheng, P. Wang, Y. Gao, Y. Wu, W. Liu, J. Ma, H. Li and S. Wu, *Org. Lett.*, 2008, **10**, 5015; (*b*) S. Sirilaksanapong, M. Sukwattanasinitt and P. Rashatasakhon, *Chem. Commun.*, 2012, **48**, 293; (*c*) P. J. Yang, H. C. Chu, T. C. Chen and H. C. Lin, *J. Mater. Chem.*, 2012, **22**, 12358.

28 J. Li, Y. Wu, F. Song, G. Wei, Y. Cheng and C. Zhu, *J. Mater. Chem.*, 2012, **22**, 478.

29 L. Xue, Q. Liu and H. Jiang, *Org. Lett.*, 2009, **11**, 3454.

30 (*a*) G. Grynkiewcz, M. Poenie and R. Y. Tsein, *J. Biol. Chem.*, 1985, **260**, 3440; (*b*) D. Maity and T. Govindaraju, *Chem. Commun.*, 2012, **48**, 1039.

31 (*a*) M. H. Ha-Thi, M. Penhoat, D. Drouin, M. Blanchard-Desce, V. Michelet and I. Leray, *Chem.–Eur. J.*, 2008, **14**, 5941; (*b*) M. Schaferling, *Angew. Chem., Int. Ed.*, 2012, **51**, 3532.

32 (*a*) Q. Zhao, F. Li and C. Huang, *Chem. Soc. Rev.*, 2010, **39**, 3007; (*b*) H. N. Kim, W. X. Ren, J. S. Kim and J. Yoon, *Chem. Soc. Rev.*, 2012, **41**, 3210.

33 (*a*) P. D. Beer and P. A. Gale, *Angew. Chem., Int. Ed.*, 2001, **40**, 486; (*b*) G. Zhang, D. Zhang, S. Yin, X. Yang, Z. Shuai and D. Zhu, *Chem. Commun.*, 2005, 2161; (*c*) S. K. Arya and S. Bhansali, *Chem. Rev.*, 2011, **111**, 6783.

34 (*a*) H. Tong, Y. Hong, J. W. Y. Lam, Y. Dong, Y. Dong, M. H. lussler, H. H. Y. Sung, Z. Li, I. D. Williams and B. Z. Tang, *J. Phys. Chem. B*, 2007, **111**, 11817; (*b*) A. Ciupa, M. F. Mahon, P. A. De Bank and L. Caggiano, *Org. Biomol. Chem.*, 2012, **10**, 8753; (*c*) J. Hatai, S. Pal, G. P. Jose, T. Sengupta and S. Bandyopadhyay, *RSC Adv.*, 2012, **2**, 7033.

35 (*a*) K. Cammann, U. Lemke, A. Rohen, J. Sander, H. Wilken and B. Winter, *Angew. Chem., Int. Ed. Engl.*, 1991, **30**, 516; (*b*) B. Ma, F. Zeng, F. Zheng and S. Wu, *Chem.–Eur. J.*, 2011, **17**, 14844; (*c*) M. Hecht, W. Krausb and K. Rurack, *Analyst*, 2013, **138**, 325.

